JACS
JOURNAL OF THE AMERICAN CHEMICAL SOCIETY
pubs.acs.org/JACS
Article

Mechanistic Insights into Fast Charging and Discharging of the Sodium Metal Battery Anode: A Comparison with Lithium

Yiren Zhong, Qiuwei Shi, Chongqin Zhu, Yifang Zhang, Min Li, Joseph S. Francisco,* and Hailiang Wang*

Cite This: J. Am. Chem. Soc. 2021, 143, 13929−13936
Read Online
ACCESS | Metrics & More | Article Recommendations | Supporting Information

ABSTRACT: Na metal anode receives increasing attention as a low-cost alternative to Li metal anode for the application in high energy batteries. Despite extensive research efforts to improve the reversibility and cycle life of Na metal electrodes, their rate performance, i.e. electrochemical plating and stripping of Na metal at high current, is underexplored. Herein, we report that Na metal electrodes, unlike the more widely studied Li metal electrodes which survive high current density up to 20 mA/cm^2, cannot be fast charged or discharged in common ether electrolyte. The fast charging, namely metal plating, is comprised by severe side reactions that decompose electrolyte into electrochemically inactive Na(I) solid species. The fast discharging, namely metal stripping, is disabled by local Na removal that deteriorates the electrical contact with the current collector. While the fast charging failure is permanent, the capacity loss from fast discharging can be recovered through a restructuring process at a low discharging current which rebuilds the electrical connection. We further reveal that the unsatisfactory rate performance of Na metal electrodes is associated with intrinsic physicochemical properties of Na. This study delineates the mechanistic origins of Na's limitation in fast plating and stripping, and demonstrates the necessity of improving the charging and discharging rate performance of Na metal electrodes.

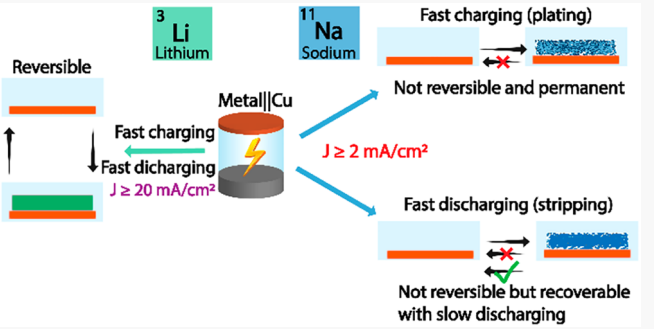

INTRODUCTION

Alkali metal batteries are considered as candidates for replacing the current Li-ion battery technology. The alkali metal anodes, with high specific capacity and low working electrode potential, enable high energy density.[1,2] For instance, Li metal, the most widely studied alkali metal anode, carries a specific capacity of 3860 mAh/g with a working potential of −3.040 V vs the standard hydrogen electrode (SHE), which leads to 10 times higher energy density than the graphite anode of current Li ion batteries.[3,4] The numbers for the Na metal anode are also promising (1164 mAh/g and −2.714 V vs SHE), making it an earth-abundant and low-cost alternative to Li.[5,6] Application of these alkali metal electrodes to batteries requires improving their Coulombic efficiency (CE) and cycling stability, which is relevant to battery cycle life. To this end, extensive research has been done to understand and resolve problems associated with side reactions and formation of metal dendrites.[7−17]

The rate performance of these metal electrodes, i.e., the part of capacity that can be retained as the electrochemical reaction rate increases, which is relevant to battery performance under fast charging and discharging conditions, is relatively overlooked. This is particularly the case for Na metal anodes, where the charging/discharging current density is generally less than 3 mA/cm^2 (Table S1).[5,17−22] Unlike in cycle life measurements where the capacity loss upon cycling is due to consumption of the metal, either by reaction with the electrolyte or forming "dead" metal, and that part becomes permanently inactive to further cycling,[7,8] the capacity reduction as the charging/discharging rate increases has a kinetic origin[23] and that part of capacity can be recovered when the current density is lowered, as established in Li/Na ion battery studies.[24−27] Therefore, studying the rate performance of alkali metal electrodes is both interesting and desirable.

In this work, we investigate the fast charging and discharging behaviors of Li and Na metal electrodes in state-of-the-art ether-based electrolytes and reveal the difference in rate performance between these two metals (Figure 1). Li metal electrodes show reversible charging and discharging in a wide current density range up to 20 mA/cm^2. Deposited Li metal maintains a densely packed structure, which can be completely removed (i.e., oxidized to Li^+) upon fast discharging. In

Received: June 30, 2021
Published: August 19, 2021

https://doi.org/10.1021/jacs.1c06794
J. Am. Chem. Soc. 2021, 143, 13929−13936

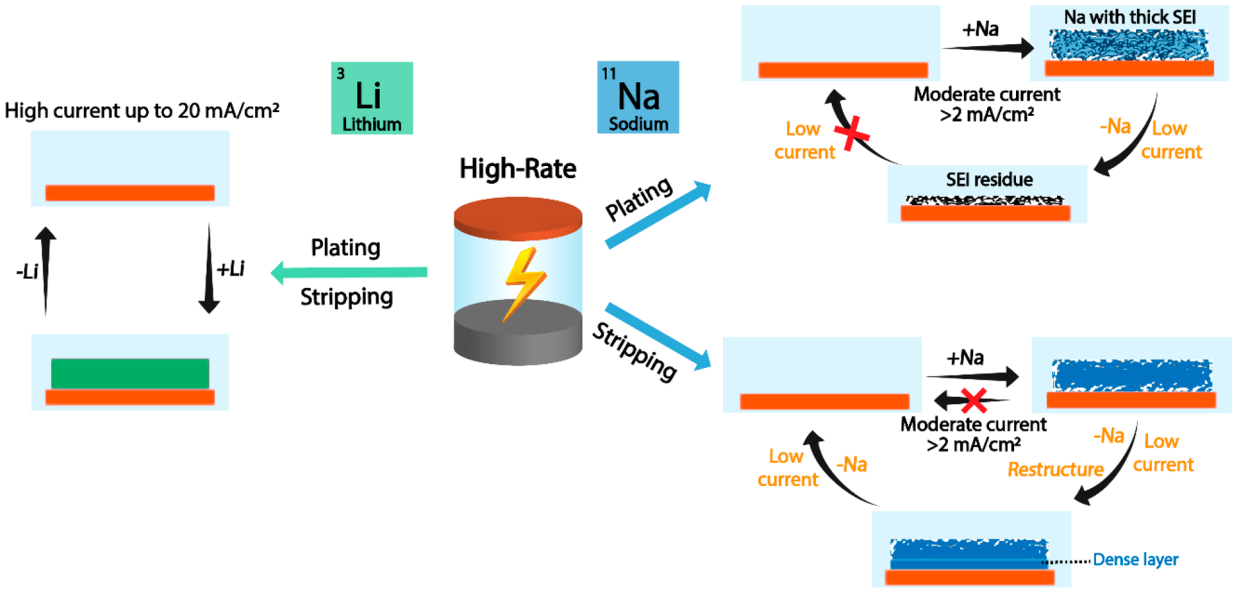

Figure 1. Schematic illustration of the difference in rate performance between Li and Na metal electrodes.

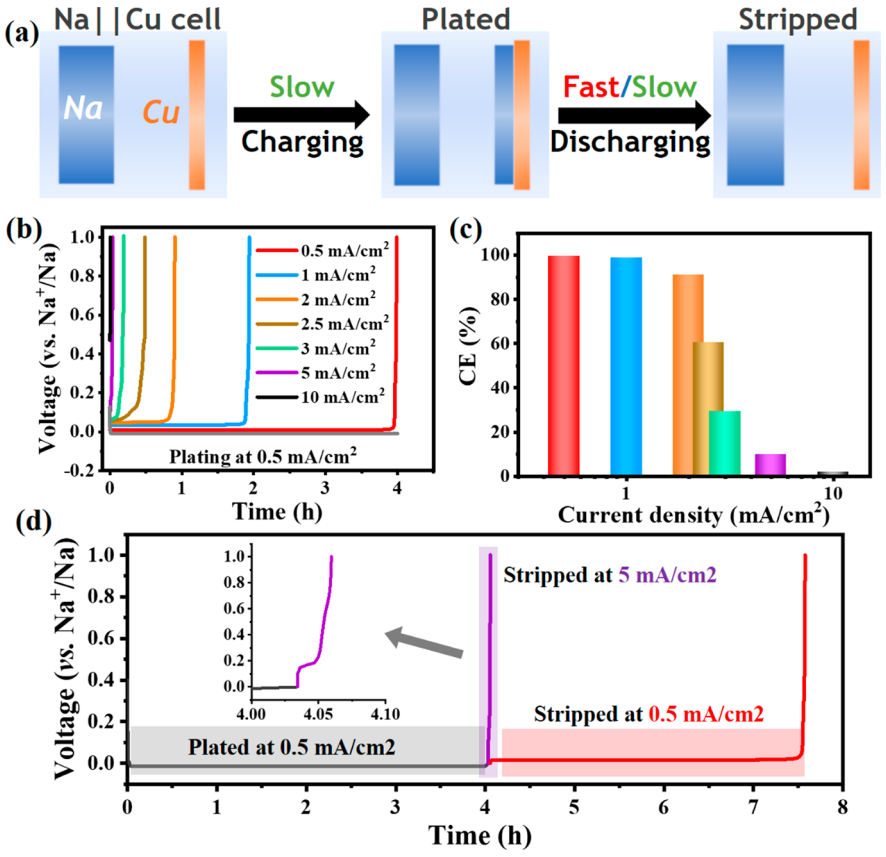

Figure 2. (a) Schematic illustration for the rate performance measurements of Na metal electrodes. (b) Voltage profiles and (c) CEs of Na||Cu cells charged at 0.5 mA/cm^2 and then discharged at different current densities. (d) Voltage profiles of Na||Cu cell charged at 0.5 mA/cm^2, discharged at 5 mA/cm^2 and then at 0.5 mA/cm^2. The capacity of each charging is 2 mAh/cm^2.

contrast, Na metal electrodes cannot be effectively charged or discharged when the current is >2 mA/cm^2. When charged at low rates, deposited Na has a whisker-like microstructure with fragile electrical connection. The conductive path can be easily cut off by the coarsening effect of Na stripping even at a moderate current. The resulting inactive Na metal, however, is not permanently "dead". It can be reactivated through rebuilding the electrical connection via restructuring at a low stripping current. Density functional theory (DFT) calculations suggest that the detrimental stripping behavior of Na originates from its lower surface energy and stripping energy compared to Li. When charged at high rates, deposited Na contains a large amount of permanently inactive ionic Na

https://doi.org/10.1021/jacs.1c06794
J. Am. Chem. Soc. 2021, 143, 13929−13936

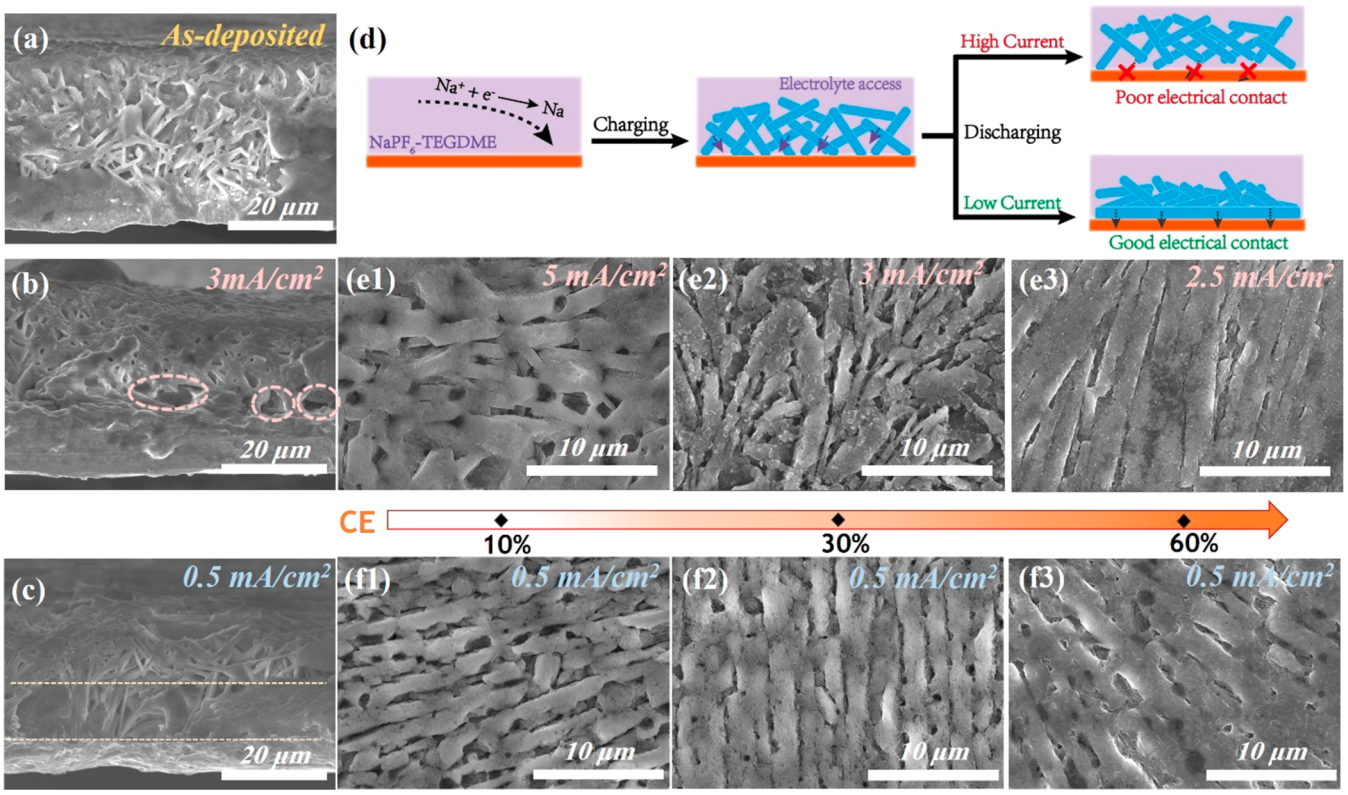

Figure 3. Cross-section SEM images of Na on Cu (a) as deposited at 0.5 mA/cm^2, (b) after stripping at 3 mA/cm^2, and (c) stripped at 0.5 mA/cm^2 to a CE cutoff of 30%. (d) Schematic illustration of Na plating-stripping process at different current densities. Top-view SEM images of Na on Cu (e1−e3) after stripping at 5, 3, and 2.5 mA/cm^2 and (f1−f3) after stripping at 0.5 mA/cm^2 to the CE cut-offs of 10%, 30%, and 60%.

species from electrolyte decomposition, causing the electrode to fail.

RESULTS AND DISCUSSION

We first examine the plating/stripping behavior of Na metal in a Na||Cu cell with 1 M $NaPF_6$ in tetraethylene glycol dimethyl ether (TEGDME) as the electrolyte. Discharged and charged with a capacity of 2 mAh/cm^2 at 0.5 mA/cm^2, a current density that is frequently employed in the cycling evaluation of Na metal batteries,[5,20] the cell delivers a high CE of 99.5% and the deposited Na film shows a smooth surface with metallic luster (Figure S1). The ease of achieving high CE in ether electrolyte without using additives is an advantage of Na anode in comparison with Li.[28] To investigate the discharging rate performance, Na||Cu cells are tested using a protocol where the current of charging, i.e., metal plating, is kept constant at 0.5 mA/cm^2 and the current of the following discharging step, i.e., metal stripping, is varied from 0.5 to 10 mA/cm^2 (Figure 2a). The cells show normal stripping behaviors with flat discharging voltage plateaus and >90% CEs at 2 mA/cm^2 or lower current densities (Figure 2b,c). At higher current densities, the discharging overpotential increases considerably (Figure 2b) with increased charge transfer resistance revealed by electrochemical impedance spectroscopy (Figure S2), indicating larger kinetic barriers. Concomitantly, the CE declines substantially to 60% and further to almost zero (Figure 2c). Interestingly, the lost capacity in fast discharging is still usable at low rates. For example, after finishing discharging at 5 mA/cm^2 (reaching the cutoff voltage of 1 V vs Na^+/Na), the electrode can be further discharged at a low current of 0.5 mA/cm^2, which eventually recovers 93.9% of the lost capacity (Figure 2d). Moreover, we find that the low-rate discharging process reactivates the electrode for fast discharging. As shown in Figure S3, 1 h of stripping at 0.5 mA/cm^2 rejuvenates a capacity of 0.1 mAh/cm^2 that can be stripped at 5 mA/cm^2. This result indicates that the slow stripping process does not only remove Na from the electrode; it also reconstructs the remaining Na.

To understand the discharging rate performance of the Na metal anode, we monitor the Na morphology at different stages of the plating-stripping process. The scanning electron microscopy (SEM) cross-section image of the 2 mAh/cm^2 Na metal film plated at 0.5 mA/cm^2 reveals an overall thickness of ~30 μm with a whisker-like morphology (Figure 3a). This Na metal layer can be completely removed electrochemically at 0.5 mA/cm^2 with a high CE close to 100% (Figure S1), leaving behind the underlying Cu current collector (Figure S4b). When stripped with a high current density of 3 mA/cm^2, only a low CE of ~30% can be obtained (Figure 2c). The remaining film retains the whisker morphology and approximately the original thickness. Large voids and detachment near the bottom of the film is observed (Figure 3b and Figure S5), suggesting that the stripping of Na metal happens there. As a comparison, we also strip the as-deposited Na metal film at the low current of 0.5 mA/cm^2 to a cutoff CE of 30%. Despite some Na metal whiskers still visible in the SEM image, the remaining film exhibits a dense structure in the region close to the Cu current collector (Figure 3c). These results demonstrate that the as-deposited Na metal layer undergoes different structural changes during slow vs fast discharging. At low current, the bottom of the Na metal layer reconstructs into a denser structure, which reinforces the electrical contact with

https://doi.org/10.1021/jacs.1c06794
J. Am. Chem. Soc. 2021, 143, 13929−13936

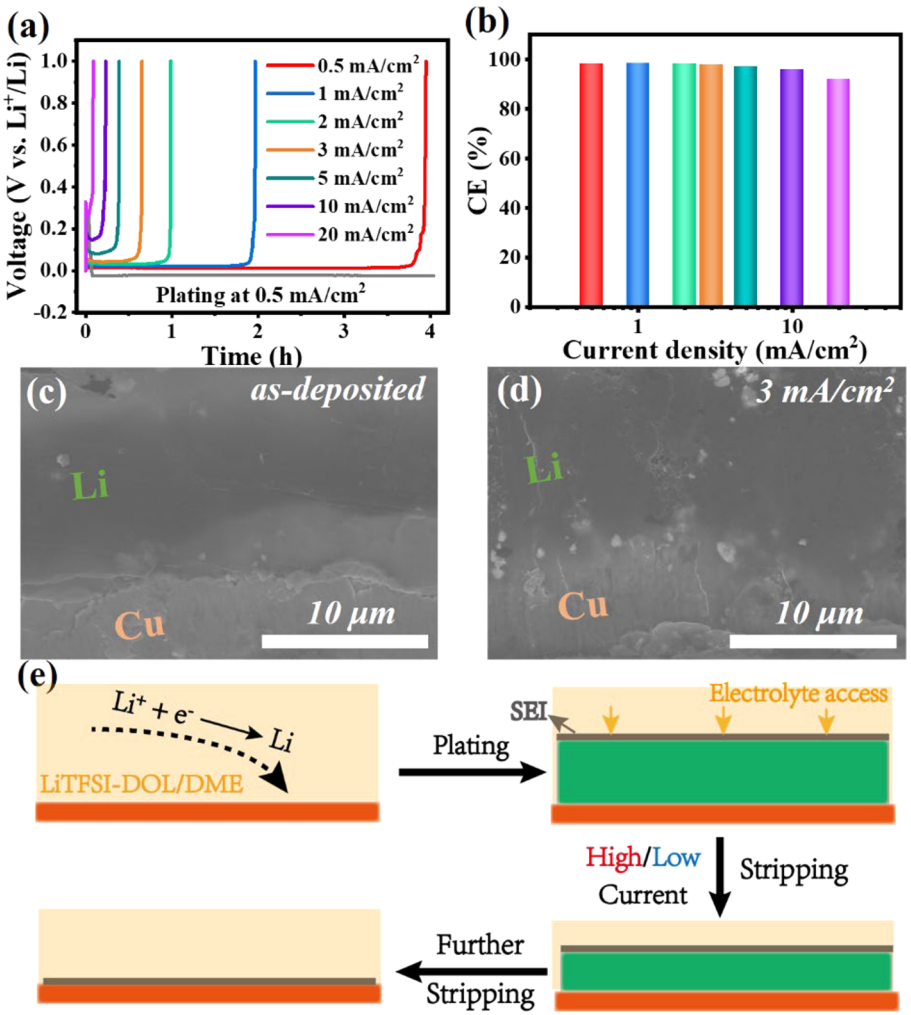

Figure 4. (a) Charging−discharging voltage profiles and (b) CEs of Li||Cu cells charged at 0.5 mA/cm^2 and discharged at different current densities. Cross-section SEM images of (c) as-deposited Li and (d) after 30% of the Li metal is removed, i.e., discharged to the CE of 30%, at 3 mA/cm^2. (e) Schematic illustration of the Li stripping process.

the Cu current collector and enables full stripping of the Na layer (Figure 3d). However, at high current, Na holds the initial whisker structure and Na stripping at the bottom results in large pinholes, which deteriorates the electrical connection between the Na layer and the Cu current collector, and thus inhibits further stripping (Figure 3d). Na stripping near Cu is possible because the porous structure of the deposited Na layer allows electrolyte penetration.

We also analyze the surface morphology of the Na metal electrodes. As-deposited Na is consisted of well-aligned long rod-like subunits with a width of ∼2 μm (Figure S4a), in line with the whisker structure identified in the cross-section images. After stripping at 5 mA/cm^2, these Na rods become short and randomly oriented (Figure 3e1). Such a less ordered microstructure may compromise the electrical contact within the Na layer, which is possibly another cause of the observed low CE. This disordering appears to be less obvious at decreased discharging current densities such as 3 and 2.5 mA/cm^2 (Figure 3e2,e3), consistent with the increased CEs. As a comparison, Na metal discharged at 0.5 mA/cm^2 does not show any sign of disordering throughout the entire stripping process (Figure 3f1−f3). Instead, the aligned Na rods tend to merge as the discharging deepens, which agrees with the densification observed in the cross-section images.

In contrast, the Li metal anode, operating in the electrolyte of 1 M lithium bis(trifluoromethanesulfonyl)imide (LiTFSI) in 1,3-dioxolane (DOL)/dimethyl ether (DME) (1:1 volumetric ratio) with 2 wt% of $LiNO_3$ additive, shows clearly different rate performance. Figure 4a,b summarizes the charging−discharging voltage profiles and CEs of Li||Cu cells subjected to fast discharging measurements up to an ultrahigh current density of 20 mA/cm^2 (CE at 40 mA/cm^2 or higher is over 100% possibly because of corrosion of the current collector, as shown in Figure S6). Impressively, Li metal electrodes survive all these conditions showing high CEs. While the discharging overpotential increases with the current, the voltage plateau is still maintained. SEM images show that as-deposited Li is a dense monolithic layer adhering well to the Cu current collector (Figure 4c), and the top surface is covered with a noticeable protective solid electrolyte interphase (SEI) layer (Figure S7).[29−31] Unlike Na, when 30% of this Li electrode is stripped at 3 mA/cm^2, the morphology/structure does not change and the close contact with the Cu substrate is maintained (Figure 4d). No structural change is visible on the top surface (Figure S8). Because of the dense structure that prevents the electrolyte from penetrating into the bulk of the electrode, Li stripping can only start from the top surface (Figure 4e). Therefore, the electrical contact between the Li

https://doi.org/10.1021/jacs.1c06794
J. Am. Chem. Soc. 2021, 143, 13929−13936

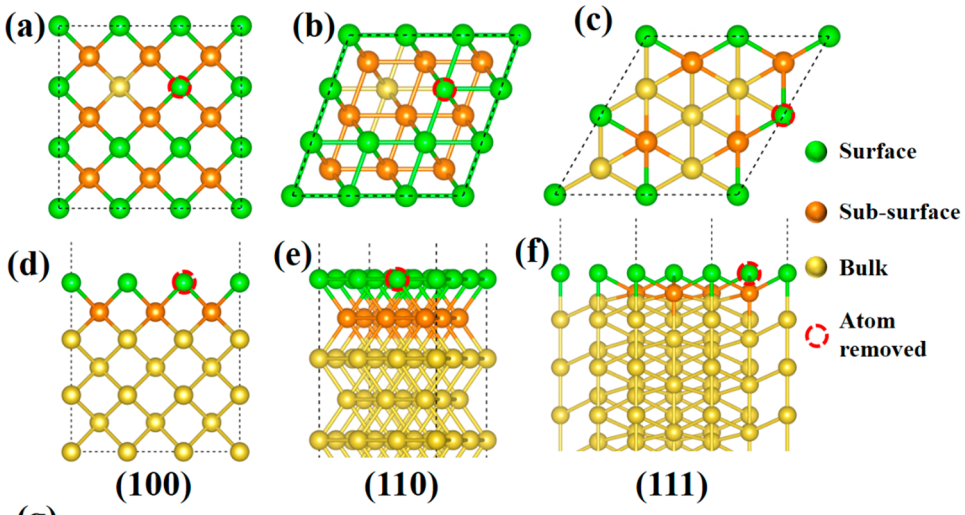

(g)

	Facet	Surface area (Å²)	Surface energy (J/m²)	Energy cost of removing one atom (eV)
Li metal	(001)	106.548	0.472	0.259
	(110)	75.341	0.475	0.192
	(111)	82.020	0.531	0.106
Na metal	(001)	158.121	0.232	0.139
	(110)	111.807	0.207	0.183
	(111)	121.720	0.260	0.106

Figure 5. (a–c) Top and (d–f) side view of different facets of bcc-structured Li or Na metal. (g) Summary of the surface area and surface energy of different facets, and the energy cost of removing one Li or Na atom from the respective surface (circled in red in a–f).

metal layer and the Cu current collector is stable, which leads to the high discharging rate performance that is not attainable by Na metal electrodes.

DFT calculations are carried out to elucidate the discharging rate performance difference between Li and Na metal electrodes. The most stable form of both metals, namely the body-centered cubic (bcc) crystal structure, is selected as the model. Surface energies are calculated for their most common facets (Figure 5a–f). We find that the surface energies of Li are generally larger than those of Na (Figure 5g), which is likely due to the smaller atomic size of Li. The lower surface energy of Na permits the formation of whisker structures with a large surface area. Li deposition, however, tends to form a dense structure to minimize the surface energy. Further, we calculate the energy cost of removing one atom from the surface of both metals to simulate the discharging process. The removal of a Li atom is more energy-consuming than that of a Na atom (Figure 5g), with a particularly sharp contrast between their most stable facets, i.e. 0.259 eV for Li (001) vs 0.183 eV for Na (110). The relatively low energy cost for Na stripping suggests that Na atoms could be easily removed at a local spot, which can explain the detrimental pinhole formation that deteriorates the electrical connection during fast discharging.

Next, we discuss the fast charging behavior of Na metal electrodes. Na||Cu cells are charged at varied current densities from 0.5 to 5 mA/cm^2 and subsequently discharged at 0.5 mA/cm^2. The increasing charging overpotential with current indicates the increasing kinetic barrier for Na plating (Figure 6a). Similar to the fast discharging case, we can observe a critical current density of 2 mA/cm^2. The CE maintains >99.5% at 2 mA/cm^2 or lower current densities and declines dramatically as the current increases beyond 2 mA/cm^2 (Figure 6b). Since a 0.5 mA/cm^2 stripping current is sufficiently slow to remove all deposited Na metal that is in good electrical contact with the Cu current collector (Figure 2), we hypothesize that the decreased CE is caused by side reactions during the plating process. To test this hypothesis, we first examine the morphology of Na metal plated at current densities >2 mA/cm^2. While the overall whisker-like morphology resembles that of Na plated at a low current density of 0.5 mA/cm^2 (Figures S9 and S10), the Na metal layer deposited at a high current density of 5 mA/cm^2 (Figure 6c1) does not have the metallic luster compared to Na plated at 0.5 mA/cm^2 (Figure 6c3), indicating that a significant portion of the layer is ionic/organic species from electrolyte decomposition. Consistently, we observe an increased charge transfer resistance (Figure S11). After the electrode is stripped at 0.5 mA/cm^2, Na metal is removed and the electrolyte decomposition products are left behind (Figure 6c2), which is different from the uniform appearance of the Cu substrate subjected to slow charging and discharging conditions (Figure 6c4).

We then resort to X-ray photoelectron spectroscopy (XPS) to analyze the composition of the deposited Na layer. The surface is mainly consisted of Na(I), as revealed by the XPS peak at the binding energy of 1072 eV in the Na 1s spectrum, regardless of the plating current (Figure 6d,e). This agrees with the existence of an SEI layer on the surface of these electrodes, which contains organic C–O and C–F species and sodium carbonate (Figure S12).[17,32,33] We further sputter the electro-

https://doi.org/10.1021/jacs.1c06794
J. Am. Chem. Soc. 2021, 143, 13929–13936

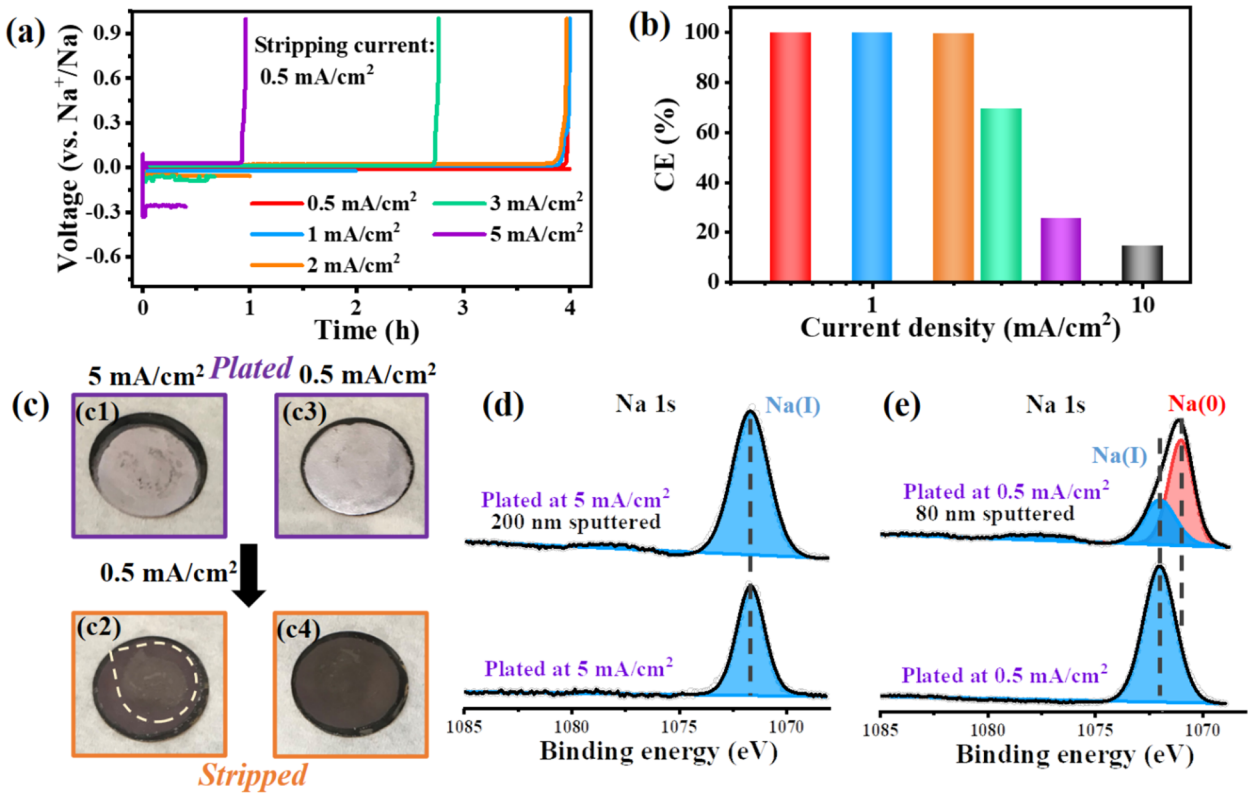

Figure 6. (a) Charging−discharging voltage profiles and (b) CEs of the Li||Cu cells charged at different current densities and then discharged at 0.5 mA/cm^2. (c) Photographs of Na (c1) deposited at 5 mA/cm^2 and then (c2) stripped at 0.5 mA/cm^2 and (c3) deposited and then (c4) stripped both at 0.5 mA/cm^2. The dash line circle in (c2) highlights accumulated electrolyte decomposition products. (d, e) XPS spectra of Na deposited at (d) 5 mA/cm^2 and (e) 0.5 mA/cm^2.

des to study the bulk composition. For the electrode charged at 0.5 mA/cm^2, a major Na(0) component is observed after only 80 nm is sputtered from the surface (Figure 6e). However, the electrode charged at 5 mA/cm^2 remains showing no sign of metallic Na even after a 200 nm layer is removed from the surface (Figure 6d), supporting our conjecture that there is severe electrolyte decomposition during the fast charging. We therefore conclude that the failure of Na metal electrodes under fast charging conditions is due to competing side reactions. A large portion of the charging electrons are consumed by electrolyte decomposition, leading to the low CEs of the fast charged cells. The extensive decomposition of electrolyte at high charging rates is possibly associated with the relatively low ionic conductivity of the Na electrolyte (1 order of magnitude lower than that of the Li electrolyte),[34−36] which cannot sustain selective Na plating at high current density. This can be understood by making a comparison to the Li case. Charging of Li metal electrodes has lower overpotential and demonstrates high CEs at fast charging rates up to 40 mA/cm^2 (Figures S13 and S14; fast charging at 80 mA/cm^2 leads to short-circuiting).

CONCLUSION

In summary, we have found that Na metal electrodes, in comparison with Li metal electrodes, show considerably lower charging and discharging rate performance. The fast discharging failure is resulted from the loss of electrical contact caused by fast stripping of Na from the bottom of the porous Na metal layer near the Cu current collector. The lost capacity can be reactivated at low stripping current density through a densification process. The fast charging performance is limited by severe electrolyte decomposition that generates a large amount of non-metallic Na species. On the basis of this understanding, we propose that approaches such as fabrication of three-dimensional electrodes and electrolyte engineering can be considered for improve the rate performance of Na metal electrodes. The former approach could help reduce the local current density and reinforce the electrical contact, whereas the latter could mitigate the side reaction problem.

ASSOCIATED CONTENT

Supporting Information

The Supporting Information is available free of charge at https://pubs.acs.org/doi/10.1021/jacs.1c06794.

Experimental and DFT calculation details, additional electrochemical, SEM and XPS characterization results, and tabulated rate performance of reported Na||Cu cells operating with ether electrolyte, including Figures S1−S14 and Table S1 (PDF)

AUTHOR INFORMATION

Corresponding Authors

Joseph S. Francisco − *Department of Earth and Environmental Sciences and Department of Chemistry, University of Pennsylvania, Philadelphia, Pennsylvania 19104, United States;* orcid.org/0000-0002-5461-1486; Email: frjoseph@sas.upenn.edu

Hailiang Wang − *Department of Chemistry, Yale University, New Haven, Connecticut 06520, United States; Energy Sciences Institute, Yale University, West Haven, Connecticut*

*06516, United States; orcid.org/0000-0003-4409-2034; Email: hailiang.wang@yale.edu

Authors

Yiren Zhong − *Department of Chemistry, Yale University, New Haven, Connecticut 06520, United States; Energy Sciences Institute, Yale University, West Haven, Connecticut 06516, United States*

Qiuwei Shi − *Department of Chemistry, Yale University, New Haven, Connecticut 06520, United States; Energy Sciences Institute, Yale University, West Haven, Connecticut 06516, United States; orcid.org/0000-0001-8543-5473*

Chongqin Zhu − *Department of Earth and Environmental Sciences and Department of Chemistry, University of Pennsylvania, Philadelphia, Pennsylvania 19104, United States*

Yifang Zhang − *Department of Chemistry, Yale University, New Haven, Connecticut 06520, United States; Energy Sciences Institute, Yale University, West Haven, Connecticut 06516, United States*

Min Li − *Materials Characterization Core, Yale University, West Haven, Connecticut 06516, United States*

Complete contact information is available at: https://pubs.acs.org/10.1021/jacs.1c06794

Notes

The authors declare no competing financial interest.

■ ACKNOWLEDGMENTS

This work was supported by the U.S. National Science Foundation (CBET-1903342). Q. Shi and Y. Zhang acknowledge exchange graduate student scholarships from the China Scholarship Council. H. Wang acknowledges the Sloan Research Fellowship. We thank Dr. Bingchen Deng and Prof. Fengnian Xia at Yale University for help with Au deposition on Cu foil.

■ REFERENCES

(1) Wang, H.; Yu, D. D.; Kuang, C. W.; Cheng, L. W.; Li, W.; Feng, X. L.; Zhang, Z.; Zhang, X. B.; Zhang, Y. Alkali Metal Anodes for Rechargeable Batteries. *Chem.* **2019**, *5*, 313−338.

(2) Xiang, J.; Yang, L.; Yuan, L.; Yuan, K.; Zhang, Y.; Huang, Y.; Lin, J.; Pan, F.; Huang, Y. Alkali-Metal Anodes: From Lab to Market. *Joule* **2019**, *3*, 2334−2363.

(3) Cheng, X. B.; Zhang, R.; Zhao, C. Z.; Zhang, Q. Toward Safe Lithium Metal Anode in Rechargeable Batteries: A Review. *Chem. Rev.* **2017**, *117*, 10403−10473.

(4) Lin, D.; Liu, Y.; Cui, Y. Reviving the Lithium Metal Anode for High-Energy Batteries. *Nat. Nanotechnol.* **2017**, *12*, 194−206.

(5) Lee, B.; Paek, E.; Mitlin, D.; Lee, S. W. Sodium Metal Anodes: Emerging Solutions to Dendrite Growth. *Chem. Rev.* **2019**, *119*, 5416−5460.

(6) Zhao, Y.; Adair, K. R.; Sun, X. Recent Developments and Insights into the Understanding of Na Metal Anodes for Na-Metal Batteries. *Energy Environ. Sci.* **2018**, *11*, 2673−2695.

(7) Zhang, Y.; Zhong, Y.; Shi, Q.; Liang, S.; Wang, H. Cycling and Failing of Lithium Metal Anodes in Carbonate Electrolyte. *J. Phys. Chem. C* **2018**, *122*, 21462−21467.

(8) Fang, C.; Li, J.; Zhang, M.; Zhang, Y.; Yang, F.; Lee, J. Z.; Lee, M. H.; Alvarado, J.; Schroeder, M. A.; Yang, Y.; et al. Quantifying Inactive Lithium in Lithium Metal Batteries. *Nature* **2019**, *572*, 511−515.

(9) Han, B.; Zou, Y.; Zhang, Z.; Yang, X.; Shi, X.; Meng, H.; Wang, H.; Xu, K.; Deng, Y.; Gu, M. Probing the Na Metal Solid Electrolyte Interphase via Cryo-Transmission Electron Microscopy. *Nat. Commun.* **2021**, *12*, 3066.

(10) Deng, Y.; Zheng, J.; Warren, A.; Yin, J.; Choudhury, S.; Biswal, P.; Zhang, D.; Archer, L. A. On the Reversibility and Fragility of Sodium Metal Electrodes. *Adv. Energy Mater.* **2019**, *9*, 1901651.

(11) Lin, D.; Liu, Y.; Li, Y.; Li, Y.; Pei, A.; Xie, J.; Huang, W.; Cui, Y. Fast Galvanic Lithium Corrosion Involving a Kirkendall-Type Mechanism. *Nat. Chem.* **2019**, *11*, 382−389.

(12) Ren, X.; Zou, L.; Cao, X.; Engelhard, M. H.; Liu, W.; Burton, S. D.; Lee, H.; Niu, C.; Matthews, B. E.; Zhu, Z.; et al. Enabling High-Voltage Lithium-Metal Batteries under Practical Conditions. *Joule* **2019**, *3*, 1662−1676.

(13) Zhang, Y.; Zhong, Y.; Liang, S.; Wang, B.; Chen, X.; Wang, H. Formation and Evolution of Lithium Metal Anode−Carbonate Electrolyte Interphases. *ACS Mater. Lett.* **2019**, *1*, 254−259.

(14) Rodriguez, R.; Loeffler, K. E.; Nathan, S. S.; Sheavly, J. K.; Dolocan, A.; Heller, A.; Mullins, C. B. In Situ Optical Imaging of Sodium Electrodeposition: Effects of Fluoroethylene Carbonate. *ACS Energy Lett.* **2017**, *2*, 2051−2057.

(15) Bai, P.; Li, J.; Brushett, F. R.; Bazant, M. Z. Transition of lithium growth mechanisms in liquid electrolytes. *Energy Environ. Sci.* **2016**, *9*, 3221−3229.

(16) Chen, X. R.; Yao, Y. X.; Yan, C.; Zhang, R.; Cheng, X. B.; Zhang, Q. A Diffusion–Reaction Competition Mechanism to Tailor Lithium Deposition for Lithium-Metal Batteries. *Angew. Chem., Int. Ed.* **2020**, *59*, 7743−7747.

(17) Seh, Z. W.; Sun, J.; Sun, Y.; Cui, Y. A Highly Reversible Room-Temperature Sodium Metal Anode. *ACS Cent. Sci.* **2015**, *1*, 449−55.

(18) Zheng, J.; Chen, S.; Zhao, W.; Song, J.; Engelhard, M. H.; Zhang, J.-G. Extremely Stable Sodium Metal Batteries Enabled by Localized High-Concentration Electrolytes. *ACS Energy Lett.* **2018**, *3*, 315−321.

(19) Shi, Q.; Zhong, Y.; Wu, M.; Wang, H.; Wang, H. High-Performance Sodium Metal Anodes Enabled by a Bifunctional Potassium Salt. *Angew. Chem.* **2018**, *130*, 9207−9210.

(20) Cui, J.; Wang, A.; Li, G.; Wang, D.; Shu, D.; Dong, A.; Zhu, G.; Luo, J.; Sun, B. Composite Sodium Metal Anodes for Practical Applications. *J. Mater. Chem. A* **2020**, *8*, 15399−15416.

(21) Wang, H.; Matios, E.; Luo, J.; Li, W. Combining Theories and Experiments to Understand the Sodium Nucleation Behavior towards Safe Sodium Metal Batteries. *Chem. Soc. Rev.* **2020**, *49*, 3783−3805.

(22) Wang, H.; Wang, C.; Matios, E.; Li, W. Critical Role of Ultrathin Graphene Films with Tunable Thickness in Enabling Highly Stable Sodium Metal Anodes. *Nano Lett.* **2017**, *17*, 6808−6815.

(23) Yu, S. H.; Huang, X.; Brock, J. D.; Abruna, H. D. Regulating Key Variables and Visualizing Lithium Dendrite Growth: An Operando X-ray Study. *J. Am. Chem. Soc.* **2019**, *141*, 8441−8449.

(24) Tian, R.; Park, S. H.; King, P. J.; Cunningham, G.; Coelho, J.; Nicolosi, V.; Coleman, J. N. Quantifying the Factors Limiting Rate Performance in Battery Electrodes. *Nat. Commun.* **2019**, *10*, 1933.

(25) Lu, J.; Chen, Z.; Pan, F.; Cui, Y.; Amine, K. High-Performance Anode Materials for Rechargeable Lithium-Ion Batteries. *Electrochem. Energy Rev.* **2018**, *1*, 35−53.

(26) Zhong, Y.; Yang, M.; Zhou, X.; Zhou, Z. Structural Design for Anodes of Lithium-Ion Batteries: Emerging Horizons from Materials to Electrodes. *Mater. Horiz.* **2015**, *2*, 553−566.

(27) Wang, H.; Yang, Y.; Liang, Y.; Cui, L. F.; Casalongue, H. S.; Li, Y.; Hong, G.; Cui, Y.; Dai, H. LiMn(1-x)Fe(x)PO4 Nanorods Grown on Graphene Sheets for Ultrahigh-Rate-Performance Lithium Ion Batteries. *Angew. Chem., Int. Ed.* **2011**, *50*, 7364−8.

(28) Zhang, Y.; Shi, Q.; Zhong, Y.; Wang, H. Intrinsically High Efficiency Sodium Metal Anode. *Sci. China: Chem.* **2020**, *63*, 1557−1562.

(29) Zhong, Y.; Lin, F.; Wang, M.; Zhang, Y.; Ma, Q.; Lin, J.; Feng, Z.; Wang, H. Metal Organic Framework Derivative Improving Lithium Metal Anode Cycling. *Adv. Funct. Mater.* **2020**, *30*, 1907579.

(30) Shi, Q.; Zhong, Y.; Wu, M.; Wang, H.; Wang, H. High-Capacity Rechargeable Batteries Based on Deeply Cyclable Lithium Metal Anodes. *Proc. Natl. Acad. Sci. U. S. A.* **2018**, *115*, 5676−5680.

(31) Zhang, X.-Q.; Chen, X.; Hou, L.-P.; Li, B.-Q.; Cheng, X.-B.; Huang, J.-Q.; Zhang, Q. Regulating Anions in the Solvation Sheath of Lithium Ions for Stable Lithium Metal Batteries. *ACS Energy Lett.* **2019**, *4*, 411−416.
(32) Le, P. M. L.; Vo, T. D.; Pan, H.; Jin, Y.; He, Y.; Cao, X.; Nguyen, H. V.; Engelhard, M. H.; Wang, C.; Xiao, J.; et al. Excellent Cycling Stability of Sodium Anode Enabled by a Stable Solid Electrolyte Interphase Formed in Ether-Based Electrolytes. *Adv. Funct. Mater.* **2020**, *30*, 2001151.
(33) Liu, W.; Chen, Z.; Zhang, Z.; Jiang, P.; Chen, Y.; Paek, E.; Wang, Y.; Mitlin, D. Lithium-Activated SnS−Graphene Alternating Nanolayers Enable Dendrite-Free Cycling of Thin Sodium Metal Anodes in Carbonate Electrolyte. *Energy Environ. Sci.* **2021**, *14*, 382−395.
(34) Cuisinier, M.; Cabelguen, P. E.; Adams, B. D.; Garsuch, A.; Balasubramanian, M.; Nazar, L. F. Unique Behaviour of Nonsolvents for Polysulphides in Lithium−Sulphur Batteries. *Energy Environ. Sci.* **2014**, *7*, 2697−2705.
(35) Sun, K.; Wu, Q.; Gan, H. Molecular Insights into Ether-Based Electrolytes for Li-FeS2 Batteries. *Energy Storage Mater.* **2018**, *12*, 85−93.
(36) Usiskin, R.; Lu, Y.; Popovic, J.; Law, M.; Balaya, P.; Hu, Y.-S.; Maier, J. Fundamentals, Status and Promise of Sodium-Based Batteries. *Nat. Rev. Mater.* **2021**, DOI: 10.1038/s41578-021-00324-w.

https://doi.org/10.1021/jacs.1c06794
J. Am. Chem. Soc. 2021, 143, 13929−13936